2004ESASP.575..241P

ON THE ROLE OF THE LARGE-SCALE MAGNETIC RECONNECTION IN THE CORONAL HEATING

Alexei A. Pevtsov$^{(1)}$ and Maria Kazachenko$^{(2)}$

$^{(1)}$National Solar Observatory at Sacramento Peak, Sunspot, NM 88349, U.S.A., Email: apevtsov@nso.edu
$^{(2)}$NSO 2004 Summer Research Assistant from Saint Petersburg State University, Russia, Email: mursic@peterlink.ru

ABSTRACT

When an active region emerges, its magnetic field reconnects with the preexisting field. This localized reconnection may affect magnetic connectivity far away from the emerging region. In some cases, the entire corona readjusts its magnetic connectivity because of changes introduced by the emerging flux. We propose that such large-scale reconnection, triggered by localized changes in the magnetic connectivity, may play a role in coronal heating.

To demonstrate the validity of this mechanism, we study the evolution of an emerging active region NOAA 8131. Using SoHO/MDI full disk magnetograms and Yohkoh/SXT data, we show that as the magnetic field emerges the surrounding corona increases its brightness and temperature. The coronal enhancement in brightness consists of two components: loop-like structures and a diffuse "cloud." Several days later, SXT data show distinct loops connecting the fully developed active region 8131 with magnetic flux outside the area of emergence. We interpret these observations as a signature of coronal heating due to a large-scale reconnection process.

Key words: Sun: corona, Sun: X-rays, gamma rays; Sun: magnetic fields.

1. INTRODUCTION

When a new active region emerges into upper solar atmosphere, its magnetic field interacts with pre-existing large-scale field. Zhang & Low (2001, 2002) showed that such interaction may open up some closed bipolar fields or even affect the polarity reversal of global magnetic field. Furthermore, the reconnection between two magnetic systems may result in heating of large-scale corona on local (i.e., above the emerging region, Shibata et al., 1991) and global scales. As new flux grows, local reconnection changes the topology of magnetic fields in vicinity of emerging region. This local change may induce re-adjustment of the coronal magnetic fields farther away. This re-adjustment creates dissipating electric currents and provides additional heating of solar corona around emerging (or evolving) active region. There is observational evidence to support the above scenario. For example, it is not uncommon to see new coronal loops developing between new active region and its surroundings (e.g., Longcope, this proceedings; see also Figure 4 in Pevtsov, 2000). Pevtsov & Acton (2001) reported significant increase in brightness of solar corona associated with emergence of a single active region. Moore et al. (2002) studied brightness of coronal loops in the vicinity of a new flux emergence site. They observed episodic increase in brightness of coronal loops not directly associated with the emerging flux.

In the present paper, we provide further support for remote coronal heating via relaxation or reconnection between large-scale pre-existing magnetic field and newly emerging active region. We demonstrate that the effects of remote heating can be seen at significant distances from the site of emergence.

2. DATA ANALYSIS

We study emerging active region (AR) NOAA 8131 using full disk magnetograms (1.98" per pixel, 96 minutes time cadence) from the SOHO Michelson Doppler Imager (MDI, Scherrer et al., 1995) and Yohkoh Soft X-ray Telescope (SXT, Tsuneta et al., 1991) observations. The data set spans seven days from January 9–16, 1998 and consists of 44 magnetogram-SXT image pairs.

MDI magnetograms were co-aligned with SXT full-resolution (1.23" per pixel) images. Next, we calculated centers of gravity (weighted by flux) of positive and negative polarities of emerging region and computed polarity separation and average center of active region. In addition, we computed total area of active region, unsigned flux, and imbalance. Only pixels with relatively strong magnetic fields, $|B_{cut}| \geq 100$ G, were used in these calculations. B_{cut} was reduced to 50 G (and in a few instances to 25 G) when there were no pixels above 100 G. For each MDI magnetogram, we selected one closest (within one hour) pair of SXT images observed in two different filters: Al.1 and AlMg, within 300 sec of each other. The SXT Al.1/AlMg filter ratio was used to compute emission measure (EM) and coronal plasma temperature (T). SXT data were corrected for the telescope point-spread function (PSF) using "sxt_decon.pro" procedure from the SolarSoft IDL library. We used the program's default PSF consisting of the delta-function core and scattering wings as determined from behind-limb observations of several X-ray flares (David McKenzie, private communication).

The temperature calculations require SXT images to be background subtracted. Typically, the background is selected from an area of faint corona in a vicinity of bright coronal loops. However, since we are interested in plasma properties of this faint corona surrounding emerging region, we cannot subtract it as a background. Thus, we do not subtract any background in temperature calcu-

Proceedings of the SOHO 15 Workshop - Coronal Heating, St. Andrews, Scotland, 6-9 September 2004
(ESA SP-575, December 2004)

lation shown on Figure 4. For temperature maps shown on Figure 7 we selected background at very low brightness area near South-East boundary of subarea. In this particular case, we did not notice significant difference in temperatures between background corrected and uncorrected data. Within these uncertainties, our numerical estimates of coronal temperature and emission measure should be treated with a caution. On the other hand, the trends in T and EM should not be affected.

To study spatial extent of coronal brightness around emerging region, we select 36 squares (5 by 5 pixels in size) situated around center of active region spaced at 10° azimuthal intervals. These calculations are done for three different distances of 5, 10, and 15 heliographic degrees, accordingly. The measurements from 18 of these squares (for each of three tested distances) are used to compute average magnetic flux, imbalance, X-ray flux, emission measure, and temperature. We use only 18 squares collectively forming a semicircle on North-East-South side of AR 8131 to exclude bright corona of AR 8132 (see Figure 2).

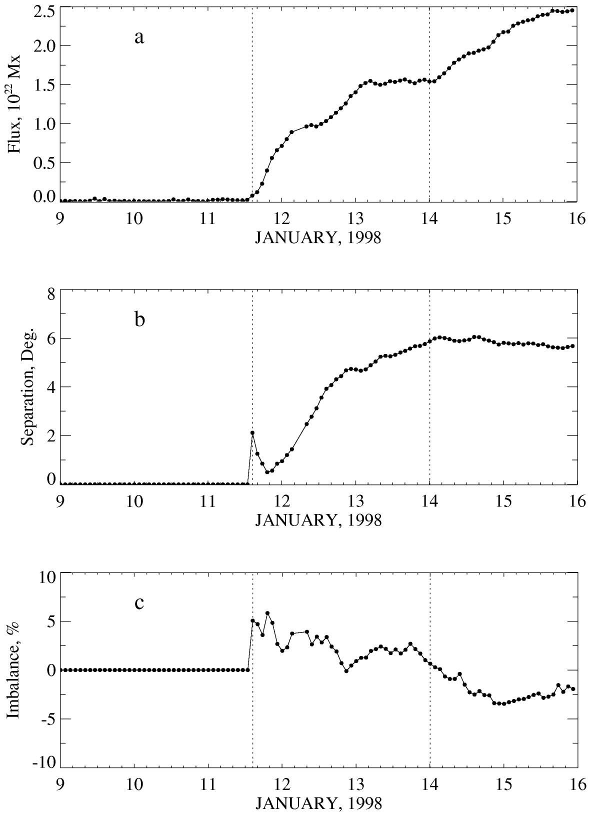

Figure 1. Total unsigned magnetic flux, polarity separation, and imbalance in AR 8131. Vertical dotted lines show approximate time of beginning of flux emergence and when the polarity separation reached a plateau. Polarity separation and imbalance are set to zero for fluxes $< 5 \times 10^{20}$ *Mx.*

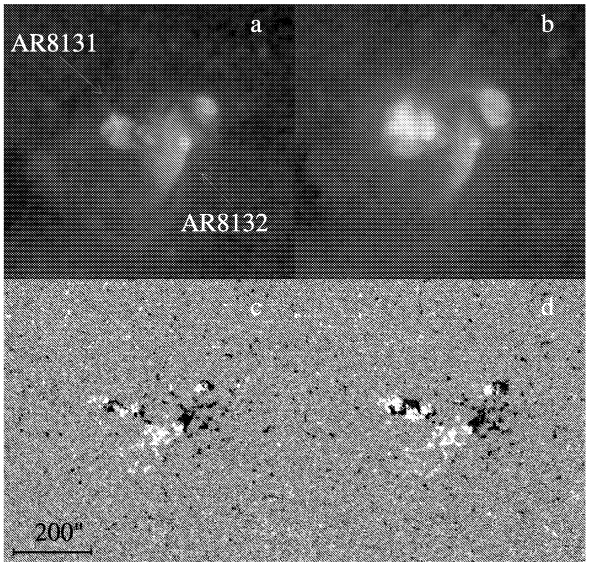

Figure 2. Magnetic field (lower panels) and X-ray images (Al.1, upper panels) of ARs 8131 and 8132. a). 11 January 1998, 16:08:01 UT, b). 12 January 1998, 00:12:55 UT, c). 11 January 1998, 16:00:04 UT, d). 12 January 1998, 00:00:04 UT.

3. EVOLUTION OF MAGNETIC FIELD AND CORONA IN AR 8131

Evolution of magnetic field and X-ray corona in AR 8131 is shown in a movie accompanying this article. AR 8131 emerged about 8.5×10^4 km (7 heliographic degrees) East and 7.3×10^4 km (6 heliographic degrees) North of the magnetic remnants of dissipating AR 8132. MDI magnetograms show first sign of flux emergence on 11 January at about 11:12 UT; heliographic coordinates of area of emergence are S22E23. By 14:24 UT on 14 January (S23W18), polarity separation reaches its maximum of about 7.3×10^4 km (6 heliographic degrees) although longitudinal flux continues to grow. Magnetic flux is well balanced throughout the period of observations. Figure 1 shows the evolution of total magnetic flux, polarity separation, and flux imbalance. In general, emerging flux exhibits a bipolar pattern; however, there is additional pattern of opposite polarities situated between two main polarities (Figure 2). This complex magnetic pattern will affect our procedure of finding the center of gravity of positive and negative polarities. For example, this might explain observed decrease in polarity separation PS at the beginning of flux emergence and some nonlinearities in PS in late stages of this active region development (Figure 1b).

Shortly after the active region emerges, surrounding corona brightens-up. Figure 2 gives example of overall changes in the corona within 8 hours of beginning of growth of AR 8131. Enhanced corona can be seen as far as ~500" from the center of AR region (Figure 3).

Comparing changes in magnetic and X-ray fluxes of areas

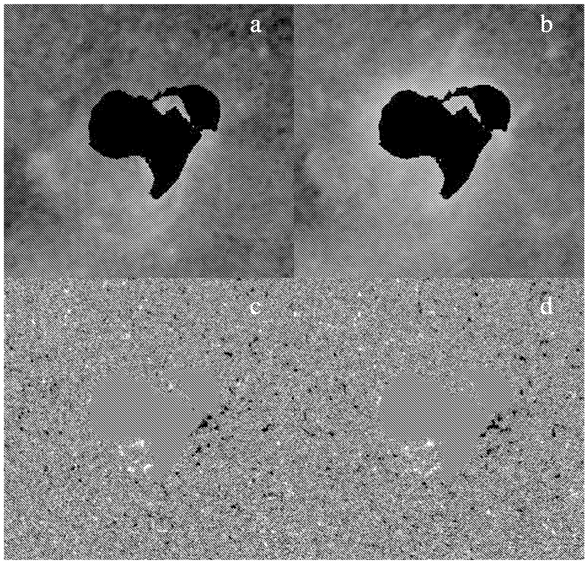

Figure 3. Same as Figure 2 with area of brightest corona masked.

Table 1. Magnetic and X-ray properties of AR8131

Object	11-JAN-98 16:08 UT	12-JAN-98 00:00 UT	Change
SXT FULL FIELD OF VIEW EXCLUDING AREA SHOWN ON FIG. 2			
X-ray, DN/s	1.21×10^7	1.18×10^7	-2.2%
M-flux, G	2.91×10^6	2.90×10^6	-0.2%
Imbalance	3.0%	5.8%	
INSIDE MASKED AREA ON FIG. 3			
X-ray, DN/s	1.07×10^6	8.81×10^6	726.5%
M-flux, G	1.03×10^5	1.52×10^5	48.1%
Imbalance	2.7%	-5.9%	
OUTSIDE MASKED AREA ON FIG. 3			
X-ray, DN/s	1.64×10^6	9.60×10^6	484.9%
M-flux, G	5.6×10^5	6.1×10^5	8.4%
Imbalance	4.2%	5.8%	

shown on Figure 3, we find that during first 8 hours, magnetic flux of AR8131 has increased by about 48% (Table 1). Brightness of coronal loops directly associated with emerging flux has increased by about seven times. On the other hand, X-ray brightness of surrounding corona has increased by nearly 5 times, and the magnetic flux of underlying area has shown only a modest increase. For comparison, magnetic and X-ray fluxes computed over entire SXT field of view (full disk and extended corona) exhibit no change.

Area of increased brightness around emerging region consists of two components: distinct loop-like structures connecting newly emerging region with surrounding weak fields and a diffuse "cloud" of enhanced corona. The brightness of the cloud is not isotropic around the region (c.f. Figure 3a and b), which suggests that the topology of surrounding magnetic field may be important. The enhancement is stronger in South-East (lower-left) direction, which supports its solar origin. Scattering on SXT mirror could not produced such highly asymmetric distribution of intensity. [1] Diffuse cloud of enhanced corona is only present during first few days of active region rapid growth; interconnecting loops became stronger with time. On January 14, SXT images show several well-developed loops connecting AR 8131 and surrounding magnetic concentrations. This evolution suggests that the origin of diffuse cloud is not unresolved loops but a heat deposited throughout the corona surrounding the emerging region.

Figure 4 shows average X-ray intensity and temperature at 5, 10, and 15 heliographic degrees from the center of emerging region. Both intensity and temperature increase as active region develops. Coronal brightness returns to pre-emergence level as polarity separation reaches maximum. On the other hand, the temperature enhancement in surrounding corona persists.

To calculate electron density (n_e) we use background-subtracted SXT Al.1 and AlMg images. Assuming $n_e \equiv constant$ over the integration volume V, $n_e = \sqrt{\frac{EM}{V}}$. Based on the extent of large-scale corona when AR 8131 crossed solar limb, we estimate the length of line-of-sight averaging L ≈ 100 pixels = 89.2 Mm, and $V \approx 7.1\times10^{25}$ cm^3. Electron densities and temperatures computed for three separate periods: before, during and after the flux emergence, are given in Table 2. Although the data show some variations in n_e, average densities are similar within 1-σ standard deviation. Hence, we conclude that the average coronal density does not change as the result of flux emergence; average $n_e \approx 1 - 1.5\times10^9$ cm^{-3}. On the other hand, average temperature is systematically higher during and after flux emergence.

The period of enhanced coronal brightness, which we attribute to the large-scale reconnection, is also associated with the period of higher flare activity in the region (Figure 5). According to the Solar Geophysical Data, first X-ray C4.5 flare occurred at 02:02 UT on 12 January. On the other hand, the coronal enhancements in brightness and temperature around AR 8131 can be seen few hours prior to this flare (Figure 6a-c and Figure 7a-c). We also note that the enhanced corona (at 10 degrees distance from the AR center) persists after the first period of flaring has ended (Figure 5). Second period of flare activity did not produce a significant enhancement in coronal brightness as compared with the first period. Thus, we argue that although flares may contribute to the enhanced brightness

---

[1] SXT data were corrected for telescope PSF as described in Section 2.

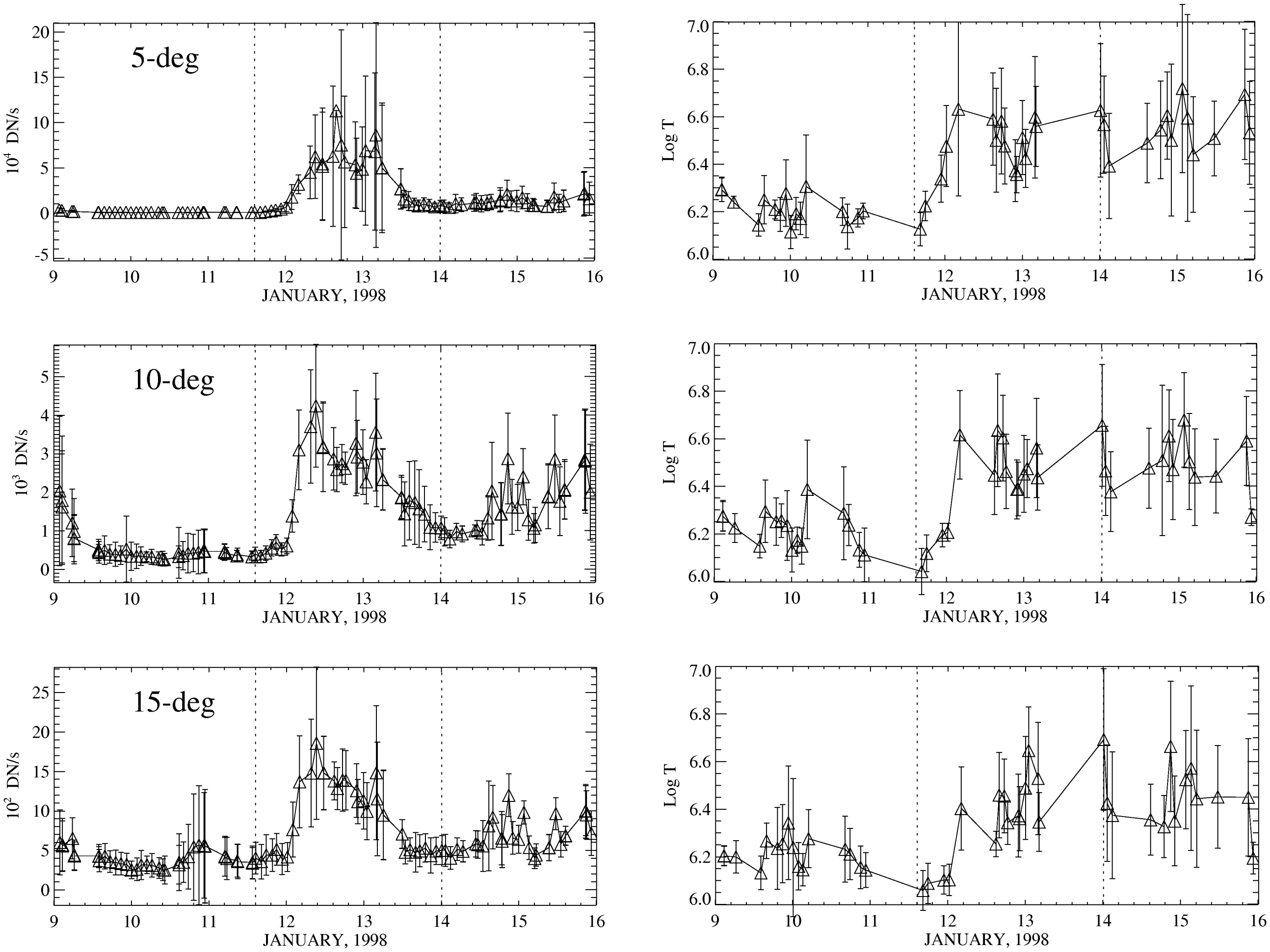

Figure 4. Average X-ray intensity (left) and temperature (right) at 5, 10, and 15 heliographic degrees from the center of emerging flux. Each data point (triangle) represents average of 18 square areas forming a semicircle on the North-East-South side of AR 8131. Error bars correspond to one standard deviation of statistical averages.

Table 2. Average Electron Density (n_e) and Temperature (Log T) around AR 8131

All dates	Before		During of AR emergence		After	
$10^9 cm^{-3}$	MK	$10^9 cm^{-3}$	MK	$10^9 cm^{-3}$	MK	$10^9 cm^{-3}$
AT 5 DEGREE DISTANCE						
2.1±0.8	6.2±0.1	1.3±0.2	6.5±0.1	3.0±1.4	6.5±0.1	2.0±0.5
AT 10 DEGREE DISTANCE						
1.4±0.3	6.2±0.1	1.2±0.3	6.4±0.2	1.1±0.5	6.5±0.1	0.8±0.3
AT 15 DEGREE DISTANCE						
1.5±0.4	6.2±0.1	1.2±0.2	6.4±0.2	1.1±0.6	6.4±0.1	0.7±0.3

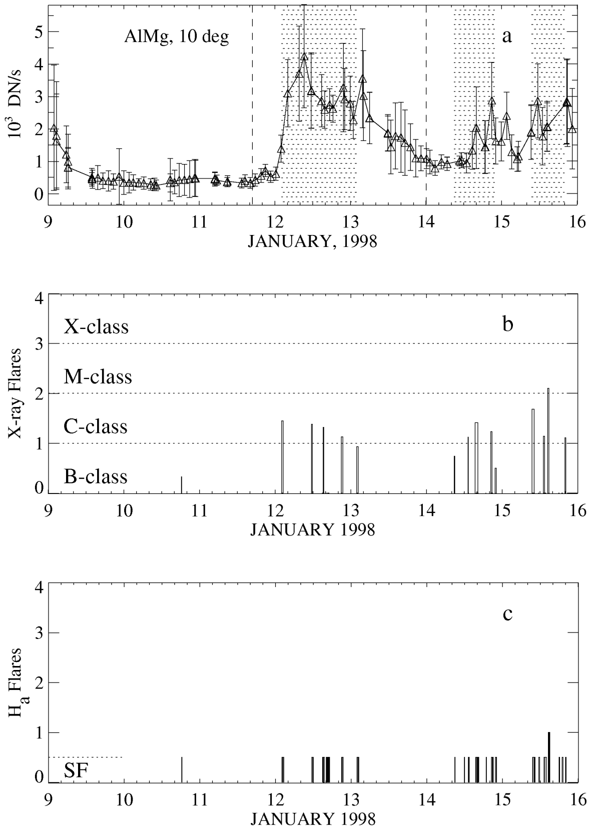

Figure 5. Average X-ray flux (upper panel) and flare activity of AR 8131. Middle panel shows X-ray flares, and lower panel is H_α flares associated with the region. Width of bins corresponds to duration of individual flares. Vertical dashed lines show the beginning of emergence of AR8131 and when the polarity separation reached a plateau. Dotted horizontal lines separate flare classes. Three dotted areas on upper panel correspond to the periods of enhanced flare activity shown on two lower panels.

of the corona, the increase in brightness on January 12–13 is associated with the flux emergence and large-scale reconnection.

Table 3 shows median values of electron density (n_e), temperature (T), and radiative loss rate (E_R) in area surrounding AR 8131 excluding active region coronal loops (masked area on Figure 3). It also provides the total thermal energy deposited in unmasked area $E_{th} = 3n_e k_b T$, where k_b is Boltzmann constant. Radiative loss rate is computed as $E_R = n_e^2 \cdot P(T)$, where radiative loss function P(T) is approximated by P(T) = $10^{-16.22}T^{-1}$ (Golub & Pasachoff, 1997). Median radiative loss rate is about $E_R \sim 3 - 8 \times 10^{-5}$ erg cm^{-3} s^{-1}, in agreement with Withbroe & Noyes (1977). E_{th} remains nearly constant during early stages of AR emergence, which may indicate continuous heating.

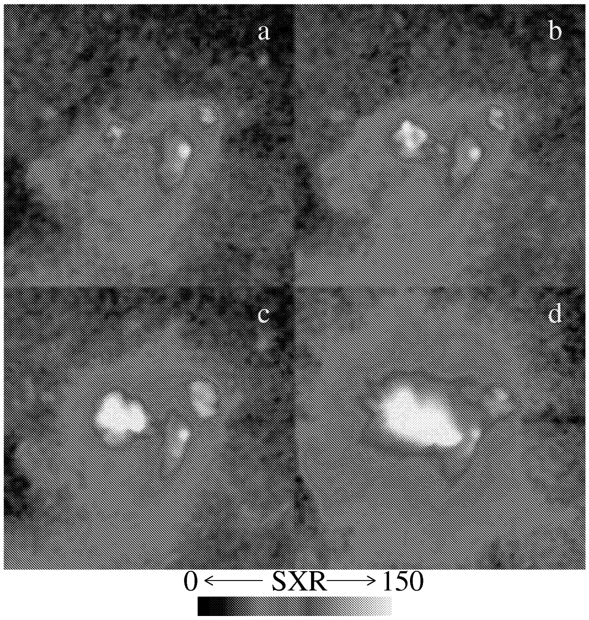

Figure 6. Coronal brightness in AlMg-filter of area shown on Figure 2 during early emergence of AR 8131. a). 11 January 1998, 16:08:01 UT; b). 11 January 1998, 17:41:49 UT; c). 12 January 1998, 00:12:55 UT; d). 12 January 1998, 03:59:13 UT. The range of scaling (in DN/sec) is shown below the Figure.

Table 3. Median Physical Parameters of Area shown on Figure 6

Panel	Log T [MK]	$n_e/10^9$ [cm^{-3}]	$E_{th}/10^{30}$ [erg]	$E_R/10^3$ [erg/(cm^3 s)]
a	6.0	1.0	2.8	0.08
b	6.1	0.9	2.6	0.04
c	6.2	0.8	2.4	0.03
d	6.3	0.9	3.3	0.03

4. CONCLUSIONS AND ADDITIONAL REMARKS

We observe significant enhancement of brightness of quiet Sun corona surrounding area of emerging active region NOAA AR8131. Area of enhancement is significantly larger than bright core loops of AR. Increase in coronal brightness is not uniform; it exhibits structures that can be interpreted as individual loops connecting emerging region with surrounding fields. The diffuse component of brightness enhancement is not isotropic, which suggests that topology of magnetic field around emerging region is important.

Although we limited the above discussion to SXT data, our preliminary results show that similar effects are present in EIT data too. However, the coronal brightness enhancement in EIT data is localized to a close proximity

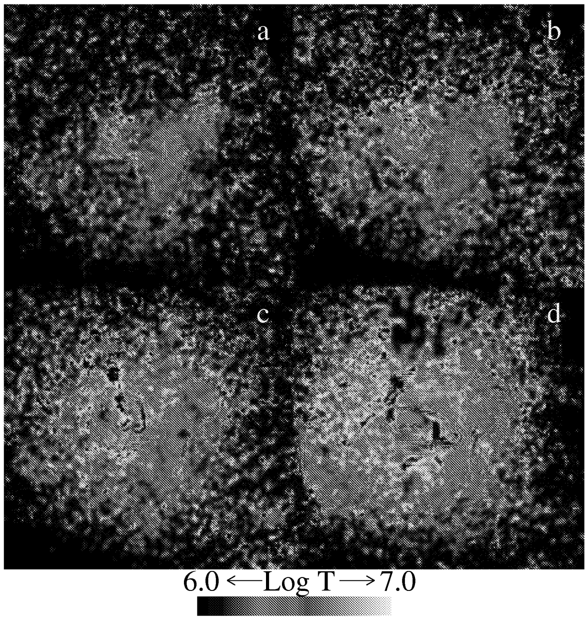

Figure 7. Coronal temperature of area shown on Figure 2 during early emergence of AR 8131. Black pixels in the middle part of active region are where the SXT_TEEM2 routine failed to converge. a). 11-JAN-98 16:08:01 UT; b). 11-JAN-98 17:41:49 UT; c). 12-JAN-98 00:12:55 UT; d). 12-JAN-98 03:59:13 UT. The range of scaling (Log T, MK) is shown below the Figure.

to AR.

Magnetic properties of quiet Sun field surrounding emerging region do not change significantly, and so, the increase in coronal brightness has no apparent connection to properties of these fields. In addition to general flux-imbalance properties, we studied the distribution of flux elements, their typical separation, and horizontal motions. We did not find significant difference in these properties prior to AR emergence and after that.

Some coronal enhancement may correlate with flare activity. Decoupling the contribution of flares and AR emergence effects requires further study.

ACKNOWLEDGEMENTS

National Solar Observatory (NSO) is operated by the Association of Universities for Research in Astronomy Inc. (AURA) under cooperative agreement with the National Science Foundation. The Yohkoh Soft X-ray Telescope was a collaborative project of the Lockheed Palo Alto Research Laboratory, the National Astronomical Observatory of Japan, and the University of Tokyo, supported by NASA and ISAS. SoHO is a project of international cooperation between ESA and NASA.

REFERENCES

Golub L. and Pasachoff J. M. *The Solar Corona*. Cambridge University Press, 1997.

Moore R. L., Falconer D. A., and Sterling A. C., Contagious Coronal Heating from Recurring Emergence of Magnetic Flux, In Martens P. and Cauffman D., editors, *Multi-Wavelength Observations of Coronal Structure and Dynamics*, Vol.13 of *COSPAR Colloquia Series*, pages 39–41, Pergamon, Dordrecht, 2002.

Pevtsov A. A., Transequatorial Loops in the Solar Corona, *ApJ*, Vol.531, 553–560, 2000.

Pevtsov A. A. and Acton L. W., Soft X-ray Luminosity and Photospheric Magnetic Field in Quiet Sun, *ApJ*, Vol.554, 416–423, 2001.

Scherrer P. H., et al., The Solar Oscillations Investigation - Michelson Doppler Imager, *Solar Phys.*, Vol.162, 129–188, 1995.

Shibata, K., et al., Atmospheric Heating in Emerging Flux Regions, In Ulmschneider, P., Priest, E., and Rosner, R., editors, *Mechanisms of Chromospheric and Coronal Heating*, pages 609–614, Springer-Verlag, Berlin, 1991.

Tsuneta S., et al., The Soft X-ray Telescope for the Solar-A Mission, *Solar Phys.*, Vol.136, 37–67, 1991.

Withbroe G. L. and Noyes R. W., Mass and Energy Flow in the Solar Chromosphere and Corona, *ARA&A*, Vol.15, 363–387, 1977.

Zhang M. and Low B. C., Magnetic Flux Emergence into the Solar Corona. I. Its Role for the Reversal of Global Coronal Magnetic Fields, *ApJ*, Vol.561, 406–419, 2001.

Zhang M. and Low B. C., Magnetic Flux Emergence into the Solar Corona. II. Global Magnetic Fields with Current Sheets, *ApJ*, Vol.576, 1005–1017, 2002.